2017-01-10

Two independent S-phase checkpoints regulate appressorium-mediated plant infection by the rice blast fungus Magnaporthe oryzae

Oses-Ruiz, M

10.1073/pnas.1611307114
Proceedings of the National Academy of Sciences
Proceedings of the National Academy of Sciences

Two independent S-phase checkpoints regulate appressorium-mediated plant infection by the rice blast fungus *Magnaporthe oryzae*

Míriam Osés-Ruiz[a], Wasin Sakulkoo[a], George R. Littlejohn[a], Magdalena Martin-Urdiroz[a], and Nicholas J. Talbot[a,1]

[a]School of Biosciences, University of Exeter, Exeter EX4 4QD, United Kingdom

Edited by Joan Wennstrom Bennett, Rutgers University, New Brunswick, NJ, and approved November 30, 2016 (received for review July 11, 2016)

To cause rice blast disease, the fungal pathogen *Magnaporthe oryzae* develops a specialized infection structure called an appressorium. This dome-shaped, melanin-pigmented cell generates enormous turgor and applies physical force to rupture the rice leaf cuticle using a rigid penetration peg. Appressorium-mediated infection requires septin-dependent reorientation of the F-actin cytoskeleton at the base of the infection cell, which organizes polarity determinants necessary for plant cell invasion. Here, we show that plant infection by *M. oryzae* requires two independent S-phase cell-cycle checkpoints. Initial formation of appressoria on the rice leaf surface requires an S-phase checkpoint that acts through the DNA damage response (DDR) pathway, involving the Cds1 kinase. By contrast, appressorium repolarization involves a novel, DDR-independent S-phase checkpoint, triggered by appressorium turgor generation and melanization. This second checkpoint specifically regulates septin-dependent, NADPH oxidase-regulated F-actin dynamics to organize the appressorium pore and facilitate entry of the fungus into host tissue.

fungi | pathogen | *Pyricularia* | appressorium | cell cycle

To cause disease, many plant-pathogenic fungi elaborate specialized infection structures called appressoria. These are swollen, dome-shaped cells that adhere tightly to the plant cell surface, where they develop turgor and bring about rupture of the host cell using mechanical force, or focused secretion of lytic enzymes. The rice blast fungus, *Magnaporthe oryzae*, has emerged as a valuable experimental model for understanding the biology of appressorium formation (1–3). Rice blast disease claims up to 30% of the annual rice harvest (4) and is therefore a significant global problem. Understanding appressorium development in this organism has the potential to lead to better rice blast disease control, by being able to target the earliest stages of plant infection.

In this study, we set out to investigate the control of appressorium development by means of cell-cycle regulation. Rice blast infections start when a three-celled conidium of *M. oryzae* lands on the rice leaf surface and germinates to form a highly polarized germ tube. The germ tube elongates and becomes flattened against the plant surface, before forming a hooked tip (5). A single round of mitosis then occurs, and one daughter nucleus migrates into the swollen germ tube tip (6). Growth at the germ tube tip then ceases, and the tip swells isotropically, resulting in formation of a dome-shaped appressorium. A thick layer of melanin is synthesized in the appressorium cell wall, and glycerol rapidly accumulates inside the cell. At the same time, the spore collapses, and its nuclei are degraded by autophagy, with the entire spore contents being trafficked to the appressorium (6). These coupled processes generate enormous hydrostatic turgor in the appressorium, measured at up to 8.0 MPa (7, 8). When maximum turgor is achieved, the appressorium undergoes dynamic remodeling of its actin cytoskeleton to form a toroidal F-actin network at the base of the cell. Septin GTPases scaffold cortical F-actin to the appressorium pore, from which a rigid penetration peg emerges to rupture the leaf cuticle (5, 9). This process requires the Nox2 NADPH oxidase complex, which regulates septin assembly and F-actin remodeling to the point of plant infection (10).

Previous work demonstrated that appressorium formation in *M. oryzae* is linked to a single round of mitosis that is always observed before cellular differentiation (11). Early appressorium development requires the nucleus in the germinating conidial cell to undergo DNA replication. Exposure to a DNA replication inhibitor—hydroxyurea (HU), for example—or generation of a temperature-dependent mutant in the regulatory subunit of the Dbf4–Cdc7 kinase complex, $\Delta nim1^{ts}$, completely arrests development of an appressorium (11). How this cell-cycle control point operates, however, is not understood. Subsequent entry into mitosis is also clearly necessary for appressorium maturation; a temperature-sensitive $\Delta nimA^{ts}$ mutant blocked at the G2-M boundary develops nonmelanized appressoria that cannot cause disease (6). Blocking the cell cycle by impairment of the anaphase-promoting complex, using a $\Delta bimE^{ts}$ mutant, or preventing mitotic exit by generating mutants expressing stabilized B-type cyclins also prevents appressorium maturation and plant infection, highlighting the need for fungal mitosis to precede plant infection (11).

In this study, we set out to investigate precisely how cell-cycle control is exerted during appressorium morphogenesis by the rice blast fungus. We show here that initiation of appressorium development requires an S-phase checkpoint that operates through the DNA damage response (DDR) pathway, requiring the Cds1 kinase. By contrast, during the next cell cycle, a second S-phase checkpoint is triggered in the appressorium and is required for the cell to repolarize. This novel checkpoint is activated by turgor

Significance

Rice blast is a devastating fungal disease of cultivated rice, and its control is vital to ensure global food security. In an effort to understand how the rice blast fungus causes disease, we have investigated how the cell cycle controls the early stages of plant infection. The rice blast fungus develops a special cell, called an appressorium, to infect rice leaves. This structure generates enormous pressure, which the fungus applies as physical force to puncture the leaf surface. We have shown that a buildup of pressure in the appressorium is necessary to trigger an unusual cell-cycle checkpoint that is necessary for the appressorium to function properly. If this process is blocked, rice blast disease cannot occur.

Author contributions: M.O.-R., W.S., and N.J.T. designed research; M.O.-R., W.S., G.R.L., and M.M.-U. performed research; G.R.L. and M.M.-U. contributed new reagents/analytic tools; M.O.-R., W.S., and N.J.T. analyzed data; and M.O.-R., W.S., and N.J.T. wrote the paper.

The authors declare no conflict of interest.

This article is a PNAS Direct Submission.

Freely available online through the PNAS open access option.

[1]To whom correspondence should be addressed. Email: N.J.Talbot@exeter.ac.uk.

This article contains supporting information online at www.pnas.org/lookup/suppl/doi:10.1073/pnas.1611307114/-/DCSupplemental.

sensing and is linked to melanin biosynthesis. The appressorium S-phase checkpoint controls NADPH oxidase-activated, septin-dependent F-actin remodeling at the base of the appressorium. This process regulates penetration peg emergence and allows plant infection to occur.

Results

Appressorium Morphogenesis Is S-Phase–Regulated and Requires Activation of CDK1 by the Cyc1 B-Type Cyclin. In *M. oryzae*, appressorium morphogenesis is always preceded by a single round of mitosis, resulting in one daughter nucleus moving to the incipient appressorium and autophagic degradation of the remaining three conidial nuclei (Movie S1). To investigate the nature of the cell-cycle checkpoint governing initial appressorium morphogenesis (11), we germinated conidia in the presence of the DNA replication inhibitor HU. Exposure to HU led to development of undifferentiated germ tubes, whereas untreated conidia developed normal melanized appressoria (Fig. 1 *A* and *B*), consistent with previous observations (6, 11) and suggesting that DNA replication must occur before initiation of appressorium development. To study the temporal dynamics of cell-cycle progression during plant infection by *M. oryzae*, we expressed a Lac repressor fused with GFP that is targeted to the fungal nucleus (GFP–LacI–NLS). This gene fusion was expressed in a construct that also contained an array of 256 Lac operator repeats inserted into a single chromosomal locus in the genome (Fig. 1*C*). In this way, it is possible to observe whether cells are in the prereplicative stage (G1), in which only a single GFP punctum is observed in the nucleus, or in the postreplicative stage (S/G2), in which two closely spaced puncta are observed, one on each sister chromatid (12). We generated a *M. oryzae* strain expressing a single integration of the GFP–LacI–NLS—lacO^{X256}—and found that S-phase entry occurs in the apical conidial cell between 2 and 3 h after germination (Fig. S1).

In eukaryotic cells, progression from S phase to mitosis is driven by the activity of B-type cyclins and associated cyclin-dependent kinases (CDKs) (13). To test whether progression of S phase is mediated through activity of the B-type cyclin–CDK complex, we generated mutations in the *M. oryzae* B-type cyclin

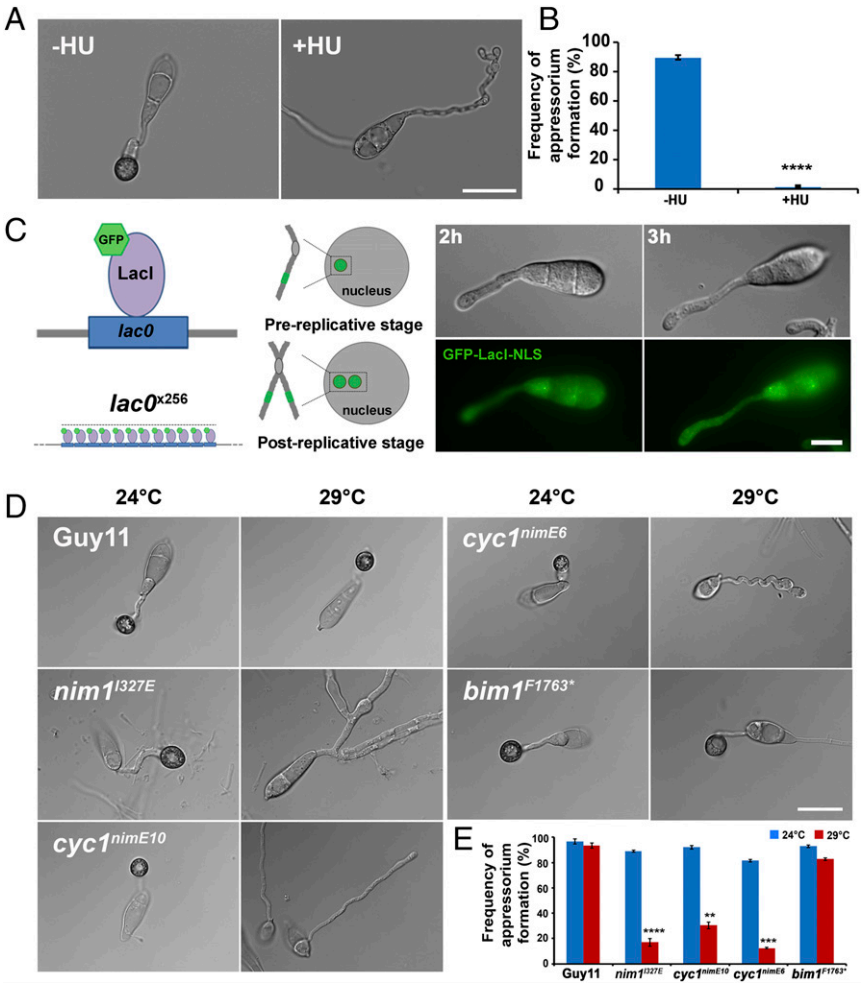

Fig. 1. Appressorium morphogenesis is an S-phase-regulated developmental process in *M. oryzae*. (*A*) Micrographs to show effect of inhibition of DNA replication by 200 mM HU on appressorium formation in *M. oryzae*, added at 2 h postinoculation (hpi) and observed at 24 h. (Scale bar, 20 μm.) (*B*) Bar chart to show frequency of appressorium formation after exposure to HU. ****$P < 0.0001$ (unpaired Student's *t* test; $n = 3$ experiments; spores = 300). (*C*) Diagram of LacO/LacI operator system. A construct containing 256 LacO repeats was integrated at a random locus in the genome. Fluorescence was visualized by expressing GFP–LacI–NLS, which binds to LacO repeats. In a prereplicative cell (G1) in which a single locus is present, a single punctum is observed, whereas in a postreplicative (S/G2) nucleus, two puncta appear. (Scale bar, 10 μm.) (*D*) Micrographs to show appressorium formation of Guy11, *nim1*^{I327E}, *cyc1*^{nimE10}, *cyc1*^{nimE6}, and *bim1*^{F1673*} mutants at 24 °C and 30 °C. (Scale bar, 20 μm.) (*E*) Bar chart to show frequency of appressorium formation by Guy11, *nim1*^{I327E}, *cyc1*^{nimE10}, *cyc1*^{nimE6}, and *bim1*^{F1673*} mutants at 24 and 30 °C. **$P < 0.01$; ***$P < 0.001$; ****$P < 0.0001$ (unpaired Student's *t* test; $n = 3$ experiments; spores observed = 300).

gene, *CYC1*, which is functionally equivalent to the *Aspergillus nidulans NIME* gene (11). In *A. nidulans*, two distinct point mutations in *NIME*, the *nimE*10 (originally identified as *nimG*10) and *nimE*6 alleles confer temperature sensitivity and distinct cell-cycle arrest in either the S or G2 phase, respectively (14–17). To test whether appressorium morphogenesis is directly dependent on activity of the CDK–cyclin B complex, we carried out targeted allelic replacements to generate $cyc1^{nimE10}$ and $cyc1^{nimE6}$ mutants, carrying S389R and F465P mutations, respectively, which are equivalent to the mutations found in the corresponding *nimE*10 and *nimE*6 of *A. nidulans* (17) (Fig. S2). These mutants carried a single targeted allelic replacement of the $cyc1^{nimE10}$ and $cyc1^{nimE6}$ alleles, confirmed by DNA sequencing, and showed severe growth defects at the semirestrictive temperature of 30 °C (Fig. S3). We evaluated the ability of these mutants to make appressoria at a semirestrictive temperature (29 °C) (Table S1). Conidia of the $cyc1^{nimE10}$ strain produced hyperpolarized germ tubes that failed to develop appressoria, whereas the $cyc1^{nimE6}$ mutant produced relatively thicker germ tubes that underwent flattening and hooking of the germ tube tip, consistent with incipient appressorium formation (Fig. 1*D*). We also analyzed a $nim1^{I327E}$ mutant, which fails to initiate DNA synthesis and instead undergoes mitotic catastrophe (11). The $nim1^{I327E}$ mutant was also unable to develop appressoria. By contrast, a $bim1^{F1763*}$ mutant, which arrests during mitosis, before anaphase, developed appressoria normally (Fig. 1*D*) (6, 11). We conclude that appressorium morphogenesis in *M. oryzae* requires an S-phase checkpoint that operates via activation of the B-type cyclin–CDK1 complex.

Appressorium Development S-Phase Checkpoint Operates Through the DDR Pathway. During DNA damage, or in the presence of unreplicated chromatin, cells are able to arrest the cell cycle by inhibitory phosphorylation of the B-cyclin–CDK1 complex. This process allows DNA repair to occur and ensure successful segregation of genetic material (18). Inhibitory phosphorylation of B-type cyclin–CDK1 complex is mediated by two serine threonine protein kinases of the DDR pathway (19). We identified a serine threonine protein kinase, Chk1, and a forkhead-associated domain-containing protein kinase, Cds1, which show 35% and 30% amino acid sequence similarity to *Saccharomyces cerevisiae* Chk1 and Rad53, respectively. To determine whether the DDR monitors DNA replication during appressorium morphogenesis, we generated targeted gene-replacement mutants, *Δchk1*, *Δcds1*, and a double *Δchk1Δcds1* mutant (Figs. S4 and S5) and then investigated the ability of these mutants to restore appressorium formation in the presence of the DNA replication inhibitor HU. We inoculated conidia of the wild-type strain Guy11 and the isogenic *Δchk1*, *Δcds1*, and *Δchk1Δcds1* mutants onto hydrophobic plastic surfaces and monitored appressorium formation at 24 h in the presence or absence of HU. In the presence of HU, both Guy11 (2.13 ± 0.63%) and the *Δchk1* null mutant (3.34 ± 2.01%) produced undifferentiated germlings and were unable to develop appressoria. By contrast, appressorium formation was restored in *Δcds1* (79.3 ± 6.73%) and *Δchk1Δcds1* (52.74 ± 7.46%) mutants (Fig. 2 *A* and *B*). However, these appressoria were nonmelanized and were able to remain intact when increasing glycerol concentrations were added in a cytorrhysis experiment (Fig. S6). This result indicates that *Δcds1* and *Δchk1Δcds1* mutants were able to bypass the S-phase arrest triggered by HU, suggesting that Chk1 and Cds1 act cooperatively to inhibit activity of the B-type cyclin–CDK and ensure successful S-phase transition during appressorium morphogenesis. The nonmelanization of appressoria that did develop in DDR mutants, however, upon continued exposure to HU, suggested that appressorium maturation also required further cell cycle-regulated processes.

A Novel S-Phase Checkpoint Regulates Plant Infection. To study mitosis during plant infection, we used live cell imaging of a Guy11 strain expressing H1-RFP (tdTomato) (11) to monitor cell-cycle progression during rice infection. We observed that, after penetration peg formation, a single round of mitosis always occurs from the single nucleus inside the appressorium (Fig. 3 *A* and *B*; and Movie S2). This finding suggests that DNA replication must occur in the appressorium before emergence of the penetration peg. To test this idea, we incubated spores of GFP–LacI–NLS strain onto hydrophobic surfaces and monitored the proportion of appressoria

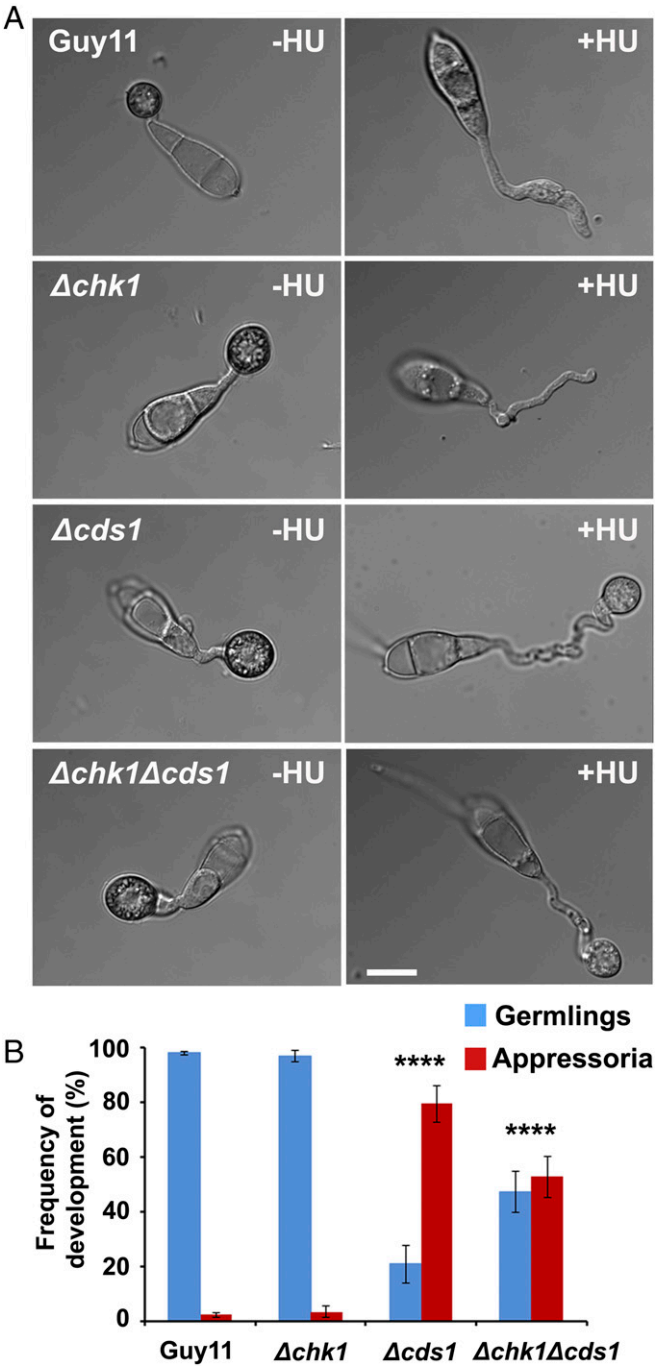

Fig. 2. An S-phase checkpoint for appressorium morphogenesis requires the DDR in *M. oryzae*. (*A*) Micrographs showing appressorium formation by Guy11, *Δchk1*, *Δcds1*, and *Δchk1Δcds1* mutants following exposure to 200 mM HU, added at 1 hpi and observed at 24 h. (Scale bar, 10 μm.) (*B*) Bar chart to show frequency of germling (blue) and appressoria (red) formation by Guy11, *Δchk1*, *Δcds1*, and *Δchk1Δcds1* mutants. ****$P < 0.0001$ (unpaired Student's *t* test; $n = 3$ experiments; spores observed = 136–601).

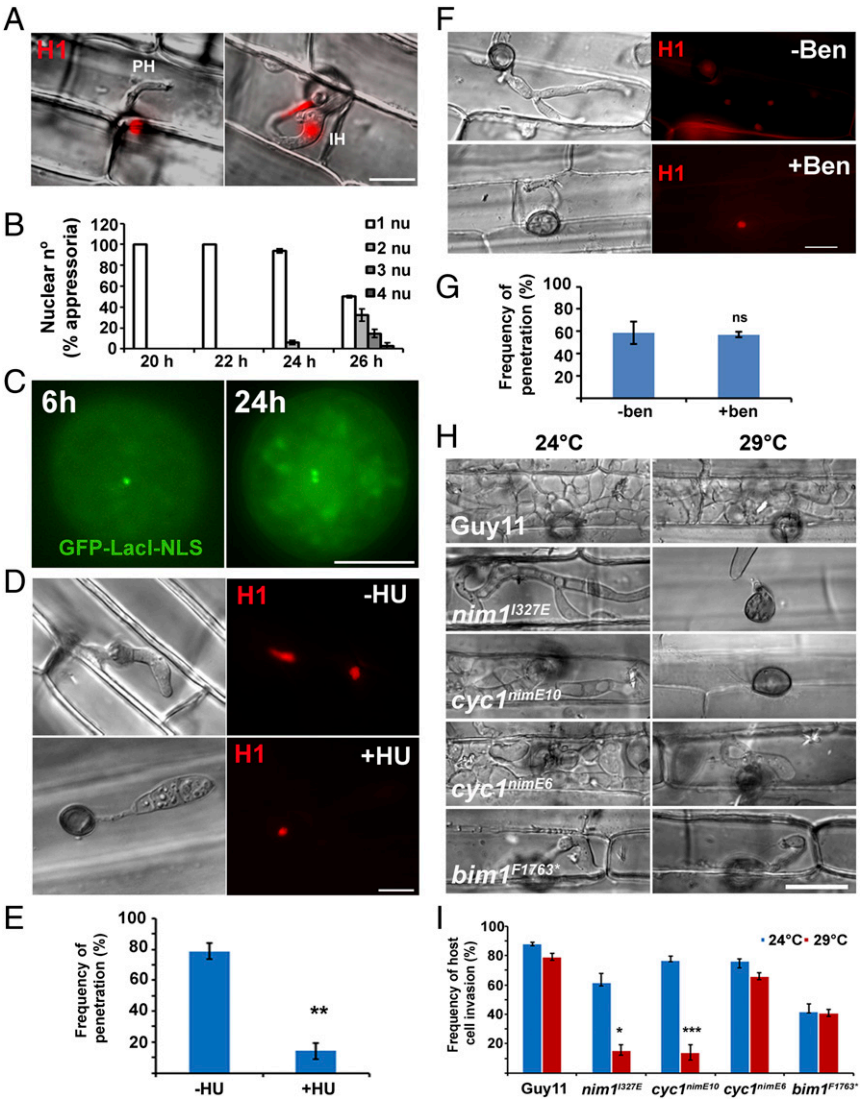

Fig. 3. Inhibition of DNA replication impairs plant infection by *M. oryzae*. (*A*) Micrographs of rice leaf sheath infection by *M. oryzae* Guy11 expressing H1-RFP. Appressoria contain a single nucleus at time of development of a penetration primary invasive hypha (PH), whereas invasive hyphae (IH) contain two nuclei. (*B*) Bar chart to show number of nuclei in appressoria and primary invasive hyphae during time course of plant infection at 20, 22, 24, and 26 h. (*C*) Micrographs to show appressorium development of Guy11 expressing GFP–LacI–NLS and LacO repeats at 6 and 24 h, showing progression from G1 to G2. (*D*) Rice leaf sheath observed 30 h after inoculation with Guy11 H1-RFP after exposure to HU at 10 h. (*E*) Bar chart to show frequency of appressoria that had formed a primary invasive hypha in the presence or absence of 1 M HU. $^{**}P < 0.01$ (unpaired Student's *t* test; $n = 3$ experiments; appressoria observed = 557–582). (*F*) Micrographs of rice leaf sheath infections of Guy11 expressing H1-RFP to show effect of a G2 arrest by exposure to benomyl (50 $\mu g \cdot mL^{-1}$). (*G*) Bar chart to show frequency of appressoria forming a penetration peg in the presence or absence of benomyl (50 $\mu g \cdot mL^{-1}$). ns, $P > 0.05$ (unpaired Student's *t* test; $n = 5$ experiments, appressoria = 479–475). (*H*) Micrographs of rice leaf sheath inoculated with Guy11, *nim1*^{I327E}, *cyc1*^{nimE10}, *cyc1*^{nimE6}, and *bim1*^{F1673*} mutants at 48 h to show effect of cell-cycle arrest points on frequency of plant infection. (Scale bar, 10 μm.) (*I*) Bar chart to show the frequency of invasion of rice leaf sheath by Guy11, *nim1*^{I327E}, *cyc1*^{nimE10}, *cyc1*^{nimE6}, and *bim1*^{F1673*} mutants at permissive (24 °C) and nonpermissive (30 °C) temperatures. $^{*}P < 0.05$; $^{***}P < 0.001$ (unpaired Student's *t* test; $n = 3$ experiments; appressoria = 138–371). (Scale bars, *A*, *D*, and *F*, 10 μm; *C*, 5 μm.)

in G1 (one punctum) and S/G2 (two puncta). We found that, after 6-h inoculation, nearly 70% of cells were in G1, whereas by 24 h after inoculation, >50% of cells had progressed to S/G2, indicating that DNA replication precedes appressorium-mediated plant infection (Fig. 3*C* and Fig. S1). We reasoned that repolarization of the appressorium leading to the formation of the penetration hypha (20) might therefore require S-phase progression. To test this idea, we first constructed a Guy11 strain expressing H1-RFP and inoculated rice leaf sheath for 10 h, after which we added HU to inhibit DNA replication. In this way, we ensured that HU would only influence events after the initial mitosis, which precedes appressorium development. When we examined rice leaf sheath infections 30 h after inoculation, we observed that in non-HU-treated infection, >80% of appressoria had successfully penetrated rice tissue and developed primary invasive hyphae. By contrast, when HU was applied, no plant infection occurred, and a single nucleus remained in the appressorium dome (Fig. 3 *D* and *E* and Fig. S7). To investigate whether the cell-cycle control point was at the G2/M boundary, we treated a Guy11 strain expressing H1-RFP with the microtubule inhibitor benomyl (50 $\mu g \cdot mL^{-1}$) and found that the frequency of primary invasive hypha formation was the same as in untreated samples, suggesting that simply exerting a mitotic block does not prevent plant infection. (Fig. 3 *F* and *G* and Fig. S8). Benomyl exposure impeded further invasive hypha development, which involves microtubule-mediated processes, but the fact that

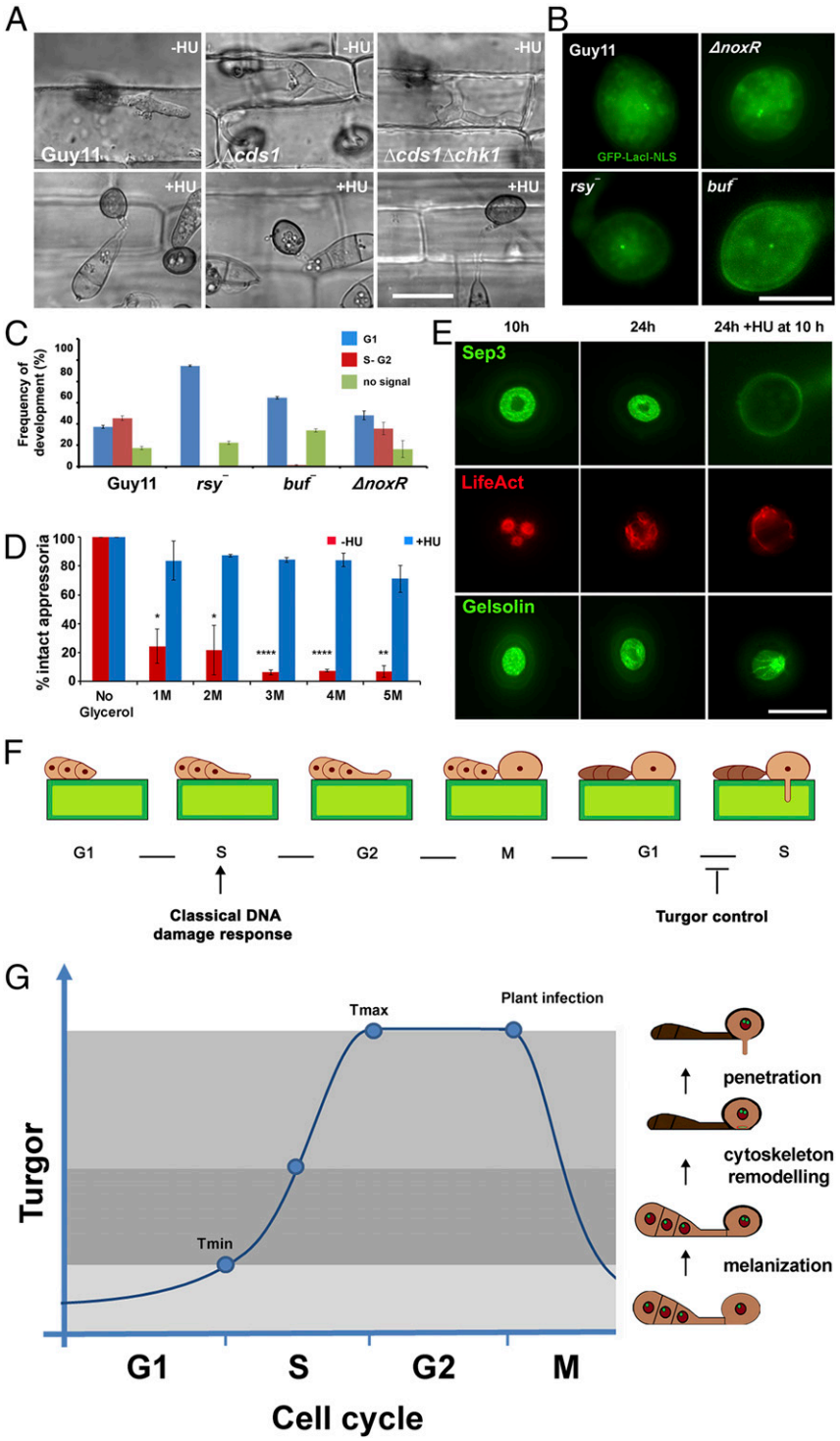

Fig. 4. S-phase regulation during plant infection is coordinated with turgor generation. (*A*) Micrograph to show rice leaf sheath inoculated with Guy11, *Δcds1*, and *Δchk1Δcds1* mutants with or without HU, added at 10 h, observed at 30 h. (Scale bar, 10 μm.) (*B*) Micrographs of Guy11, Δ*noxR*, *rsy*⁻, and *buf*⁻ mutants expressing GFP–LacI–NLS and LacO repeat construct to show effect on G1 to G2 progression. (Scale bar, 10 μm.) (*C*) Bar chart to show frequency of progression to G2 in appressoria of Guy11, Δ*noxR*, *rsy*⁻, and *buf*⁻ expressing GFP–LacI–NLS and LacO repeat construct. (*D*) Incipient cytorrhysis assay to measure appressorium turgor generation with or without HU. Appressoria were allowed to form on hydrophobic plastic coverslips for 10 h, when 200 mM HU was added. At 24 h, appressoria were exposed to increasing concentrations of glycerol, and the percentage of intact appressoria was recorded. $*P < 0.05$; $**P < 0.01$; $****P < 0.0001$ (unpaired Student's *t* test; $n = 3$ experiments; appressoria observed = 90–126). (*E*) Micrographs of Guy11 expressing Sep3–GFP, LifeAct–RFP, and Gelsolin–GFP with or without HU, added at 10 h and observed at 30 h. (Scale bar, 10 μm.) (*F*) Model depicting cell-cycle transitions necessary for appressorium-mediated plant infection by *M. oryzae*. An S-phase checkpoint operates during initial appressorium morphogenesis and depends on the DNA DDR. A second S-phase checkpoint operates during appressorium maturation and depends on cellular turgor. (*G*) Model to show cell-cycle control of rice cell entry by *M. oryzae*. A newly formed appressorium is initially arrested in G1 with a minimum turgor pressure level (Tmin). Turgor accumulates due to glycerol synthesis and melanization of the appressorium cell wall. A threshold of turgor is generated (Tmax) in the appressorium in order for S-phase entry, which is necessary for septin-dependent F-actin remodeling at the base of the appressorium. This process leads to formation of a penetration peg to rupture the plant cuticle.

primary penetration peg formation was not affected suggests that a mitotic block is not sufficient to prevent plant infection by *M. oryzae*. We then examined conditional *nim1*^{I327E}, *cyc1*^{nimE10}, *cyc1*^{nimE6}, and *bim1*^{F1763*} mutants, impaired at different cell-cycle stages. We inoculated rice leaf sheath at the permissive temperature (24 °C) and allowed them to develop for 10 h to allow completion of the first round of mitosis in the germ tube and to develop an appressorium. We then incubated them at the semirestrictive temperature (29 °C) for 30 h in total. We found that *nim1*^{I327E} and *cyc1*^{nimE10} mutants, which are defective in S-phase progression, were unable to infect rice tissue and form primary invasive hyphae at 29 °C (Fig. 3 *H* and *I*). However, *cyc1*^{nimE6} and *bim1*^{F1763*} mutants, which are arrested at G2 and preanaphase, respectively, were able to infect rice tissue and generate invasive hyphae at 29 °C (Fig. 3 *H* and *I*). Rice infection is therefore dependent on S-phase progression in the appressorium.

Turgor-Dependent S-Phase Progression Regulates Appressorium Repolarization. We next explored the nature of the S-phase checkpoint that operates during appressorium-mediated plant penetration. Because the initial S-phase checkpoint that controls appressorium morphogenesis depends on the DDR and, more specifically, the serine threonine protein kinase Cds1, we investigated whether this was the case for control of appressorium maturation. We inoculated Δ*cds1*, Δ*chk1*Δ*cds1* null mutants, and Guy11 on rice leaf sheath and exposed appressoria to HU 10 h after inoculation. Strikingly, none of the checkpoint kinase mutants were able to penetrate rice tissue in the presence of HU (Fig. 4*A* and Fig. S9). We conclude that the DDR is therefore not involved in S-phase control during appressorium maturation.

We reasoned that appressorium maturation and the control of penetration peg development therefore require an S-phase checkpoint, regulated by a distinct DDR-independent mechanism. Appressorium maturation is associated with rapid generation of enormous turgor pressure, so we decided to test whether mutants impaired in turgor generation were affected in cell-cycle control. Appressorium turgor is generated by glycerol accumulation (7) and development of a thick melanin layer in the appressorium dome. Melanin-deficient mutants, such as *rsy1*$^{-}$ and *buf1*$^{-}$, lack key enzymes for synthesis of di-hydroxynaphthalene melanin and, consequently, are nonpathogenic and do not generate appressorium turgor (8). We expressed GFP–LacI–NLS in *rsy1*$^{-}$ and *buf1*$^{-}$ mutants containing the LacO^{x256} construct integrated into their genomes at a single locus. We then monitored the DNA replication status of the appressorium nucleus and found that *rsy1*$^{-}$ and *buf1*$^{-}$ mutants are arrested in G1 with a single GFP–LacI–NLS punctum in the appressorium. By contrast, the wild type progressed through S phase normally. To test whether this effect was associated with turgor control, we then tested S-phase progression in penetration-deficient mutants that were not affected in turgor control. To perform this test, we expressed GFP–LacI–NLS in Δ*noxR* null mutants. NoxR is the p67^{phox}-like regulator of the NADPH oxidase complex that regulates septin-mediated F-actin remodeling and plant infection (10), Strikingly, Δ*noxR* penetration-deficient mutants displayed two separate puncta, like the wild-type Guy11, indicating that S-phase was able to proceed normally (Fig. 4 *B* and *C*). Our results therefore suggest that appressorium turgor generation, which requires melanin synthesis, is necessary for progression from G1 to S phase.

To investigate the interdependency of turgor control and S-phase progression, we decided to carry out an incipient cytorrhysis experiment to measure cellular turgor in the presence of the DNA-replication inhibitor HU. Cytorrhysis provides a measure of internal cellular turgor, based on the external solute concentration necessary to collapse the appressorium (7, 8). We observed that 24% (±15.6 SE) of appressoria remained intact when 1 M glycerol was applied to nontreated appressoria, whereas 71% (±7.06 SE) of intact appressoria were still observed when 5 M glycerol was applied to appressoria that had been exposed to HU (Fig. 4*D*). Moreover, appressoria that were exposed to HU exhibited a thicker melanin layer from untreated cells (Fig. S10). The DDR mutants behaved in the same way as Guy11, and we observed the same hypermelanization and increased turgor in Δ*cds1* and Δ*chk1*Δ*cds1* mutants (Fig. S10). This observation indicates that impairment of S-phase progression leads to excess turgor generation in the appressorium, which further suggests that S-phase control is necessary for turgor modulation in mature appressoria, and independent of the DDR. To test this hypothesis, we investigated the effect of S-phase progression on cytoskeleton remodeling, which is necessary for appressorium repolarization (9, 10). Appressorium function requires assembly of a heterooligomeric septin ring composed of four septin GTPases (Sep3, Sep4, Sep5, and Sep6) that scaffolds F-actin to generate a penetration peg that ruptures the plant cuticle (9, 10). We expressed Sep3–GFP, LifeAct–RFP, and Gelsolin–GFP in Guy11 and germinated conidia on hydrophobic plastic surfaces to monitor the frequency of septin and F-actin ring formation at the appressorium pore in the presence or absence of HU. In the absence of HU, a Sep3–GFP ring was always present at the base of the appressorium pore (Fig. 3*D*). In the presence of HU, however, Sep3–GFP was severely disrupted and the septin ring no longer maintained. Disruption of appressorium pore organization was also observed in LifeAct–RFP and Gelsolin–GFP expressing strains of *M. oryzae* after exposure to HU (Fig. 3*D*). Moreover when septin-dependent components of the appressorium pore (9), such as the PAK kinase Chm1, the ERM (Ezrin/Radiixin/Moesin domain) protein Tea1, the Bim1, Amphiphysin, and Rvs167 BAR domain protein, or the actin nucleation protein, Las17, were localized in the presence of HU, they all showed abnormal localization patterns (Fig. S9). Moreover, when we analyzed appressorium shape in the presence or absence of HU, we could readily distinguish that the pore was aberrantly formed in appressoria treated with HU (Fig. S10). We conclude that septin-dependent F-actin remodeling at the base of the appressorium requires S-phase progression to have taken place.

Discussion

In this work, we have shown that rice infection by the rice blast fungus is controlled by two discrete S-phase checkpoints that operate over two successive cell cycles in the fungus. One of these checkpoints operates at the initial stages of appressorium formation and is connected to the DDR pathway, whereas the second checkpoint is controlled in a completely novel manner by the prevailing turgor pressure within the appressorium.

Appressorium morphogenesis by *M. oryzae* is induced when a spore lands on a hard, hydrophobic surface and by perception of wax monomers released from the rice cuticle. Arresting the cell cycle at the S phase, either through application of HU or generation of conditional *nim1* and *cyc1* ^{nimE10} mutants affected in DNA replication, prevented formation of the hooked, terminal swelling of the germ tube from which the appressorium forms. Live cell imaging confirmed that formation of this terminal swelling is significant, because it provides the destination for the daughter nucleus, after the single round of mitosis that precedes appressorium differentiation. The S phase is therefore critical in controlling initiation of appressorium development (11).

Operation of the initial S-phase checkpoint involves the DDR, because deletion of the Cds1 kinase-encoding gene allows appressorium morphogenesis to proceed even in the presence of HU. It is increasingly apparent that the DDR interacts with the morphogenesis checkpoint and nutrient-sensing pathways (21). In *S. cerevisiae*, for example, the Cds1 homolog, Rad53, interacts with septins and Swe1, linking cytokinesis with control of DNA replication (22, 23). The cAMP-dependent protein kinase A pathway (PKA) may also interact with the DDR, because in *S. cerevisiae* PKA regulates cell-cycle progression and cell size through the RNA-binding protein Whi3 (24). In *M. oryzae*, cAMP-dependent

PKA is necessary for differentiation and cell-size control of appressoria (25).

We observed in this study that, in contrast to early appressorium development, maturation of the infection cell and, in particular, its ability to repolarize and form a penetration hypha, is regulated by a separate S-phase checkpoint. After autophagic cell death of the conidium and nuclear degeneration (6), the single nucleus in the nascent appressorium appears to be arrested at G1, based on our observations using the LacO/LacI biomarker. However, it is also clear that plant infection cannot proceed until this nucleus has passed into S phase, and, without this cell-cycle progression, the appressorium does not initiate polarized growth to infect plant cells.

Generation of a minimum turgor threshold therefore appears to be necessary for progression into S phase, because melanin-deficient mutants, which are well known to be impaired in turgor generation, form appressoria that stay arrested in G1. Preventing S-phase progression, in *cyc1*^{nimE10} mutants, or by exposure to HU, furthermore prevents septin-mediated remodeling of the F-actin cytoskeleton to the appressorium pore and organization of the nascent penetration peg. Control of septin organization and F-actin dynamics at the point of plant infection are therefore dependent on S-phase progression. These observations lead us to propose a model (Fig. 4*G*) in which a minimum turgor threshold must be achieved in the appressorium, dependent on osmolyte accumulation and melanin deposition. Achievement of this turgor threshold in the appressorium therefore regulates entry into S phase. The threshold of turgor also facilitates remodeling of the cytoskeleton, controlled by regulated synthesis of reactive oxygen species by the Nox2 complex (10), which acts on septin GTPases (9) to organize the appressorium pore, regulating membrane curvature generation, polarized exocytosis, and exocyst organization (26), followed by rapid actin polymerization to drive polarized growth of the penetration hypha into the rice cuticle.

How might such cell-cycle control operate in the appressorium? Perhaps the most useful analogy for penetration peg emergence is the control of budding in *S. cerevisiae* in which cells are initially arrested in G1 (27, 28) and the tyrosine kinase Swe1 plays an important role in monitoring cytoskeletal organization, leading ultimately to Cdc28 activation, which triggers polarized growth through activation of the guanine nucleotide exchange factor of the Cdc42 GTPase and Cdc24 (29). Components of this GTPase signaling module are direct targets of Cdc28 and control subsequent bud emergence (28). In *M. oryzae*, CDK1/cyclin complexes may also control the GTPase signaling module to direct growth toward the base of the appressorium, controlling septin and F-actin organization. The Cdc42 GTPase and its effector Chm1 (a Cla4 homolog) have, for instance, been shown to be required for cytoskeletal reorganization at the appressorium pore and for plant penetration (9, 30, 31). Cdc42 may therefore activate septin ring assembly through action of the PAK kinases Chm1 and activate F-actin remodeling through the Nox2/NoxR complex and its interaction with Rac (10, 32).

It is also apparent that S-phase progression is contingent on turgor control rather than being explicitly linked to DDR control, because deletion of Cds1 does not restore plant infection to *M. oryzae* appressoria that have been exposed to HU. Consistent with such a model, HU treatment leads to runaway turgor generation, excess melanization, and an inability to repolarize, suggesting that integrated control of DNA replication and turgor modulation is necessary for operation of the infection cell. Further analysis of mutants that are impaired only in repolarization mechanisms, but that develop turgor normally, will be necessary to confirm these predictions. Our current interpretation is made based on the investigation of defects in cell-cycle progression by melanin-deficient mutants, coupled with the lack of such effects in the *ΔnoxR* mutant, and the inability of DDR mutants to overcome the S-phase checkpoint operating within the appressorium.

When considered together, our results suggest that infection of rice tissue by *M. oryzae* requires discrete cell-cycle morphogenetic transitions to enable appressorium formation, appressorium repolarization, and cuticle rupture, thereby enabling host cell invasion. This temporal sequence of shape transitions by the fungus is tightly coordinated with nuclear division and critical to the establishment of rice blast disease.

Materials and Methods

Fungal Strains, Growth Conditions, and DNA Analysis. Storage, maintenance, and growth of *M. oryzae* strains, media composition, nucleic acid extraction, and fungal transformation were all performed as described (33). Generation of DNA fragments, gel electrophoresis, restriction enzyme digestion, gel blots, and sequencing were performed by using standard procedures (34).

Generation of *cyc1*^{nimE10}, *cyc1*^{nimE6}, Δ*chk1*, Δ*cds1*, and Δ*chk1*Δ*cds1* Mutants and Strains Expressing GFP Fusions. Details of construction for allelic replacement vectors for generating *cyc1*^{nimE10} and *cyc1*^{nimE6} mutants are given in *SI Materials and Methods*. DNA sequences were retrieved from the *M. oryzae* genome database of the Broad Institute at the Massachusetts Institute of Technology (archive.broadinstitute.org/annotation/fungi/magnaporthe/) and used to design primers (Table S2). Targeted gene replacement of *CHK1* and *CDS1* was performed by using hygromycin B (*hph*) and bialaphos (*bar*) selectable markers, respectively, by the split marker technique as described (35). The *chk1:hph* construct was introduced into Guy11, and transformants were selected on hygromycin B (200 μg·mL^{-1}). Both Guy11 and Δ*chk1* mutants were transformed with *cds1:bar* and transformants selected on glufosinate (30 μg·mL^{-1}). Transformants were assessed by Southern blot. Plasmids expressing GFP and RFP fusions were transformed into Δ*chk1*, Δ*cds1*, and Δ*chk1*Δ*cds1* mutants and single-insertion transformants selected by Southern blot. For chromosome tagging, a plasmid containing the GFP-lac repressor fusion containing a nuclear localization signal (GFL–LacI–NLS) and a plasmid containing an array of 256 lac operator repeats were cotransformed into each fungal strain and selected in the presence of glufosinate (30 μg·mL^{-1}) and secondly in the presence of chlorimuron ethyl (50 μg·mL^{-1}).

Infection Structure Development Assays, Plant Infection Assays, and Live-Cell Imaging of Nuclei and Cytoskeletal Components of *M. oryzae*. Appressorium development was induced in vitro on borosilicate 18- × 18-mm glass coverslips (Fisher Scientific U.K. Ltd.), adapted from ref. 36. A total of 50 μL of conidial suspension (5 × 10^4 mL^{-1}) was placed on a coverslip and incubated at 24 °C. Rice leaf sheath inoculations, adapted from ref. 37, were performed to observe development of invasive hyphae. At desired time points, the DNA replication inhibitor HU was added to germinating spores (200 mM) or appressoria on leaf sheaths (1 M) after removing preexisting water. Benomyl was used at a final concentration of 50 μg·mL^{-1} (6), and samples were incubated at 24 °C. Development of appressoria was observed by using an IX81 motorized inverted microscope (Olympus), and images were captured by using a Photometrics CoolSNAP HQ2 camera (Roper Scientific), under control of the MetaMorph software package (MDS Analytical Technologies). Onion epidermis assays and leaf drop experiments were performed as described (38, 39).

Laser-Scanning Confocal Microscopy of Infected Plant Tissue. A Leica SP8 laser-scanning confocal microscope equipped with a harmonic compound planar apochromatic confocal scanning (HC PC APO CS2) 63×/1.40 oil immersion lens was used to collect signal from Guy11 H1-RFP cells during infection of rice leaf sheath. RFP was excited by using a diode-pumped solid state 561-nm laser at 0.1% transmission, and emitted signal was collected from 590 to 632 nm by using the SP8 hybrid detector, with gain set to 77. Differential interference contrast images were collected by using the same laser settings and photomultiplier tube gain of 254. Movies were generated from *x,y,z,t* series (*x,y* 512 × 512 pixels; *z* step was 0.34 μm with a pinhole set to 1 arbitrary unit and taken at a frame rate of one frame every 10 min) from infected tissue samples. Data used to generate Movies S1 and S2 represents an *x,y,z,t* cropped selection from the original data file.

Accession Numbers. Sequence data from this article can be found in the GenBank/European Molecular Biology Laboratory databases (https://www.ncbi.nlm.nih.gov/genbank/) under the following accession numbers: *M. oryzae* NIM1 (MGG_00597), *M. oryzae* BIM1 (MGG_03314), *M. oryzae* CYC1 (MGG_05646), *M. oryzae* CHK1 (MGG_03729), *M. oryzae* CDS1 (MGG_04790), and *A. nidulans* NimE (AN3648).

ACKNOWLEDGMENTS. We thank Stephen A. Osmani (The Ohio State University) and Steven W. James (Gettysburg College) for providing unpublished

data regarding the specific DNA sequence changes present in the *Aspergillus nidulans nimE*10 and *nimE*6, as well as for providing these fungal strains; Jose Perez-Martin (Instituto de Biología Funcional y Genómica) for the helpful suggestions and discussions; and Yasuyuki Kubo and Fumi Fukada (Kyoto Prefectural University) for providing the LacO/LacI biomarker. This work was supported by EU-Initial Training Network Marie Curie Grant PITN-GA-2009-237936 (to M.O.-R.); a Halpin Scholarship (to W.S.); and a European Research Council Advanced Investigator award (to N.J.T.) under the European Union's Seventh Framework Programme FP7/2007-2013/ERC Grant Agreement 294702 GENBLAST (to M. M.-U. and G.R.L.).

1. Martin-Urdiroz M, Oses-Ruiz M, Ryder LS, Talbot NJ (2016) Investigating the biology of plant infection by the rice blast fungus *Magnaporthe oryzae*. *Fungal Genet Biol* 90: 61–68.
2. Talbot NJ (2003) On the trail of a cereal killer: Exploring the biology of *Magnaporthe grisea*. *Annu Rev Microbiol* 57:177–202.
3. Wilson RA, Talbot NJ (2009) Under pressure: Investigating the biology of plant infection by *Magnaporthe oryzae*. *Nat Rev Microbiol* 7(3):185–195.
4. Fisher MC, et al. (2012) Emerging fungal threats to animal, plant and ecosystem health. *Nature* 484(7393):186–194.
5. Bourett TM, Howard RJ (1990) Invitro development of penetration structures in the rice blast fungus *Magnaporthe grisea*. *Can J Bot* 68:329–342.
6. Veneault-Fourrey C, Barooah M, Egan M, Wakley G, Talbot NJ (2006) Autophagic fungal cell death is necessary for infection by the rice blast fungus. *Science* 312(5773): 580–583.
7. de Jong JC, McCormack BJ, Smirnoff N, Talbot NJ (1997) Glycerol generates turgor in rice blast. *Nature* 389:244–245.
8. Howard RJ, Valent B (1996) Breaking and entering: Host penetration by the fungal rice blast pathogen *Magnaporthe grisea*. *Annu Rev Microbiol* 50:491–512.
9. Dagdas YF, et al. (2012) Septin-mediated plant cell invasion by the rice blast fungus, *Magnaporthe oryzae*. *Science* 336(6088):1590–1595.
10. Ryder LS, et al. (2013) NADPH oxidases regulate septin-mediated cytoskeletal remodeling during plant infection by the rice blast fungus. *Proc Natl Acad Sci USA* 110(8):3179–3184.
11. Saunders DG, Aves SJ, Talbot NJ (2010) Cell cycle-mediated regulation of plant infection by the rice blast fungus. *Plant Cell* 22(2):497–507.
12. Straight AF, Belmont AS, Robinett CC, Murray AW (1996) GFP tagging of budding yeast chromosomes reveals that protein-protein interactions can mediate sister chromatid cohesion. *Curr Biol* 6(12):1599–1608.
13. Coudreuse D, Nurse P (2010) Driving the cell cycle with a minimal CDK control network. *Nature* 468(7327):1074–1079.
14. Morris NR (1976) Nucleosome structure in *Aspergillus nidulans*. *Cell* 8(3):357–363.
15. Bergen LG, Upshall A, Morris NR (1984) S-phase, G2, and nuclear division mutants of *Aspergillus nidulans*. *J Bacteriol* 159(1):114–119.
16. O'Connell MJ, Osmani AH, Morris NR, Osmani SA (1992) An extra copy of nimEcyclinB elevates pre-MPF levels and partially suppresses mutation of nimTcdc25 in Aspergillus nidulans. *EMBO J* 11(6):2139–2149.
17. James SW, et al. (2014) Restraint of the G2/M transition by the SR/RRM family mRNA shuttling binding protein SNXAHRB1 in *Aspergillus nidulans*. *Genetics* 198(2):617–633.
18. Rhind N, Russell P (1998) Mitotic DNA damage and replication checkpoints in yeast. *Curr Opin Cell Biol* 10(6):749–758.
19. Sanchez Y, et al. (1999) Control of the DNA damage checkpoint by chk1 and rad53 protein kinases through distinct mechanisms. *Science* 286(5442):1166–1171.
20. Park G, Xue C, Zheng L, Lam S, Xu JR (2002) MST12 regulates infectious growth but not appressorium formation in the rice blast fungus *Magnaporthe grisea*. *Mol Plant Microbe Interact* 15(3):183–192.
21. de Sena-Tomás C, Fernández-Álvarez A, Holloman WK, Pérez-Martín J (2011) The DNA damage response signaling cascade regulates proliferation of the phytopathogenic fungus *Ustilago maydis* in planta. *Plant Cell* 23(4):1654–1665.
22. Enserink JM, Smolka MB, Zhou H, Kolodner RD (2006) Checkpoint proteins control morphogenetic events during DNA replication stress in *Saccharomyces cerevisiae*. *J Cell Biol* 175(5):729–741.
23. Smolka MB, et al. (2006) An FHA domain-mediated protein interaction network of Rad53 reveals its role in polarized cell growth. *J Cell Biol* 175(5):743–753.
24. Wang H, Garí E, Vergés E, Gallego C, Aldea M (2004) Recruitment of Cdc28 by Whi3 restricts nuclear accumulation of the G1 cyclin-Cdk complex to late G1. *EMBO J* 23(1): 180–190.
25. Xu JR, Hamer JE (1996) MAP kinase and cAMP signaling regulate infection structure formation and pathogenic growth in the rice blast fungus *Magnaporthe grisea*. *Genes Dev* 10(21):2696–2706.
26. Gupta YK, et al. (2015) Septin-dependent assembly of the exocyst is essential for plant infection by *Magnaporthe oryzae*. *Plant Cell* 27(11):3277–3289.
27. Bishop AC, et al. (2000) A chemical switch for inhibitor-sensitive alleles of any protein kinase. *Nature* 407(6802):395–401.
28. McCusker D, et al. (2007) Cdk1 coordinates cell-surface growth with the cell cycle. *Nat Cell Biol* 9(5):506–515.
29. Howell AS, et al. (2012) Negative feedback enhances robustness in the yeast polarity establishment circuit. *Cell* 149(2):322–333.
30. Li L, Xue C, Bruno K, Nishimura M, Xu JR (2004) Two PAK kinase genes, CHM1 and MST20, have distinct functions in *Magnaporthe grisea*. *Mol Plant Microbe Interact* 17(5):547–556.
31. Zheng W, et al. (2009) A Cdc42 ortholog is required for penetration and virulence of *Magnaporthe grisea*. *Fungal Genet Biol* 46(6-7):450–460.
32. Chen J, et al. (2008) Rac1 is required for pathogenicity and Chm1-dependent conidiogenesis in rice fungal pathogen *Magnaporthe grisea*. *PLoS Pathog* 4(11):e1000202.
33. Talbot NJ, Ebbole DJ, Hamer JE (1993) Identification and characterization of MPG1, a gene involved in pathogenicity from the rice blast fungus *Magnaporthe grisea*. *Plant Cell* 5(11):1575–1590.
34. Sambrook J, Fritsch EF, Maniatis T (1989) *Molecular Cloning: A Laboratory Manual* (Cold Spring Harbour Lab Press, Cold Spring Harbor, NY), 2nd Ed.
35. Sweigard JA, Carroll AM, Farrall L, Chumley FG, Valent B (1998) *Magnaporthe grisea* pathogenicity genes obtained through insertional mutagenesis. *Mol Plant Microbe Interact* 11(5):404–412.
36. Hamer JE, Howard RJ, Chumley FG, Valent B (1988) A mechanism for surface attachment in spores of a plant pathogenic fungus. *Science* 239(4837):288–290.
37. Kankanala P, Czymmek K, Valent B (2007) Roles for rice membrane dynamics and plasmodesmata during biotrophic invasion by the blast fungus. *Plant Cell* 19(2): 706–724.
38. Chida T, Sisler HD (1987) Restoration of appressorial penetration ability by melanin precursors in *Pyricularia oryzae* treated with antipenetrants and in melanin-deficient mutants. *J Pestic Sci* 12:49–55.
39. Jia Y, Valent B, Lee FN (2003) Determination of host responses to *Magnaporthe grisea* on detached rice leaves using a spot inoculation method. *Plant Dis* 87:129–133.

Supporting Information

Osés-Ruiz et al. 10.1073/pnas.1611307114

SI Materials and Methods

Construction of the *M. oryzae cyc1*^{niEG10} and *cyc1*^{nimE6} Gene Replacement Vectors. The partial length of *A. nidulans nimE* gene was amplified from *A. nidulans nimE10* (previously named *nimG10*) and *nimE6* and an isogenic wild-type strain (provided by Steve W. James, Gettysburg College, Gettysburg, PA). The *A. nidulans nimE10* and *nimE6* alleles were amplified (primers NIME-P1 and -P2) and sequenced to reveal point mutations. The *A. nidulans nimE10* allele contains a serine residue altered to arginine at position 369. The *nimE6* allele has a leucine residue mutated to proline at position 445.

In-fusion cloning based on in vitro homologous recombination was performed to generate temperature-sensitive alleles of *M. oryzae*, by using a commercial kit (In-Fusion Cloning Kit; Clontech Laboratories, Inc.). The *cyc1*^{nimE10} and *cyc1*^{nimE6} alleles carry S389R and F465P mutations, respectively, equivalent to the corresponding *A. nidulans* mutants. For generating the *cyc1*^{nimE10} allele, the *CYC1* gene (genomic locus MGG_05646) was amplified in two fragments. A 1.3-kb *CYC1* fragment (primers V-BamHI-nimG11_P1 and Mut-nimG11_P2) and a 0.5-kb *CYC1* fragment (primers Mut-nimG11_P3 and Hyg-nimG11_P4) were amplified with either side of the region requiring nucleotide substitution and have 15-base pair overhangs complementary to the adjacent fragment. Substitution of codon 389 from serine (AGC) to arginine (CGC) was introduced to the 0.5-kb *CYC1* fragment by primers Mut-nimG11_P3. A 1.4-kb hygromycin-resistance cassette *HPH* was amplified from pCB1004 by using primers M13F and M13R. A 1.0-kb 3′ untranslated region (3′ UTR) downstream of the *CYC1* locus was amplified (primers Hyg-nimG11-3UTR_P5 and V-BamHI-nimG11-3UTR_P6) to provide a region homology 3′ to the *HPH* cassette in the gene replacement vector. Four inserts, including the 1.3- and 0.5-kb fragments of the *CYC1* gene, the *HPH* cassette, and the 3′ UTR, were cloned into a HindIII-cut *1284 pNEB-Nat-Yeast* cloning vector.

For the *cyc1*^{nimE6} allele, a 1.6-kb *CYC1* fragment (primers V-BamHI-nimG11_P1 and Mut-nimE6_P2) and a 178-bp *CYC1* fragment (primers Mut-nimE6_P3 and Hyg-nimG11_P4) were amplified. Substitution of codon 465 from phenylalanine (TTC) to proline (CCT) was introduced to the 178-bp *CYC1* fragment by primer Mut-nimE6_P3. Four inserts, including the 1.6-kb and 178-bp fragments of the *CYC1* gene, the *HPH* cassette, and the 3′ UTR, were cloned into a HindIII-cut *1284 pNEB-Nat-Yeast* cloning vector. The *cyc1*^{nimE10} and *cyc1*^{nimE6} constructs were excised by BamHI to generate the full-length 4.2-kb gene replacement constructs and transformed into the Guy11 wild-type strain.

Melanin Thickness Quantification and Appressorium Pore Formation Analysis. Appressorium development was induced in vitro as described. A total of 50 μL of conidial suspension (5×10^4 mL^{-1}) were placed on a borosilicate glass coverslip and incubated at 24 °C. After 10 h, 200 mM DNA replication inhibitor HU was added. At 24 hpi, images of appressoria were obtained as described. To quantify the melanin layer thickness, appressoria were sampled by using random procedures, and images were analyzed by using the MetaMorph software package (MDS Analytical Technologies). Appressoria formed attached to the surface of the glass coverslips, which ensured measurements of the medium section. Statistical analysis was performed by using Prism7 (GraphPad) software. Datasets were compared by using the nonparametric Kruskal–Wallis test and represented by scatter dot plot (mean ± SE). To compare the formation of the appressorium pore with or without HU, intensity profile values were measured over line scan diameters that crossed the center of the appressorium in Guy11, *Δcds1*, and *Δchk1Δcds1* mutants.

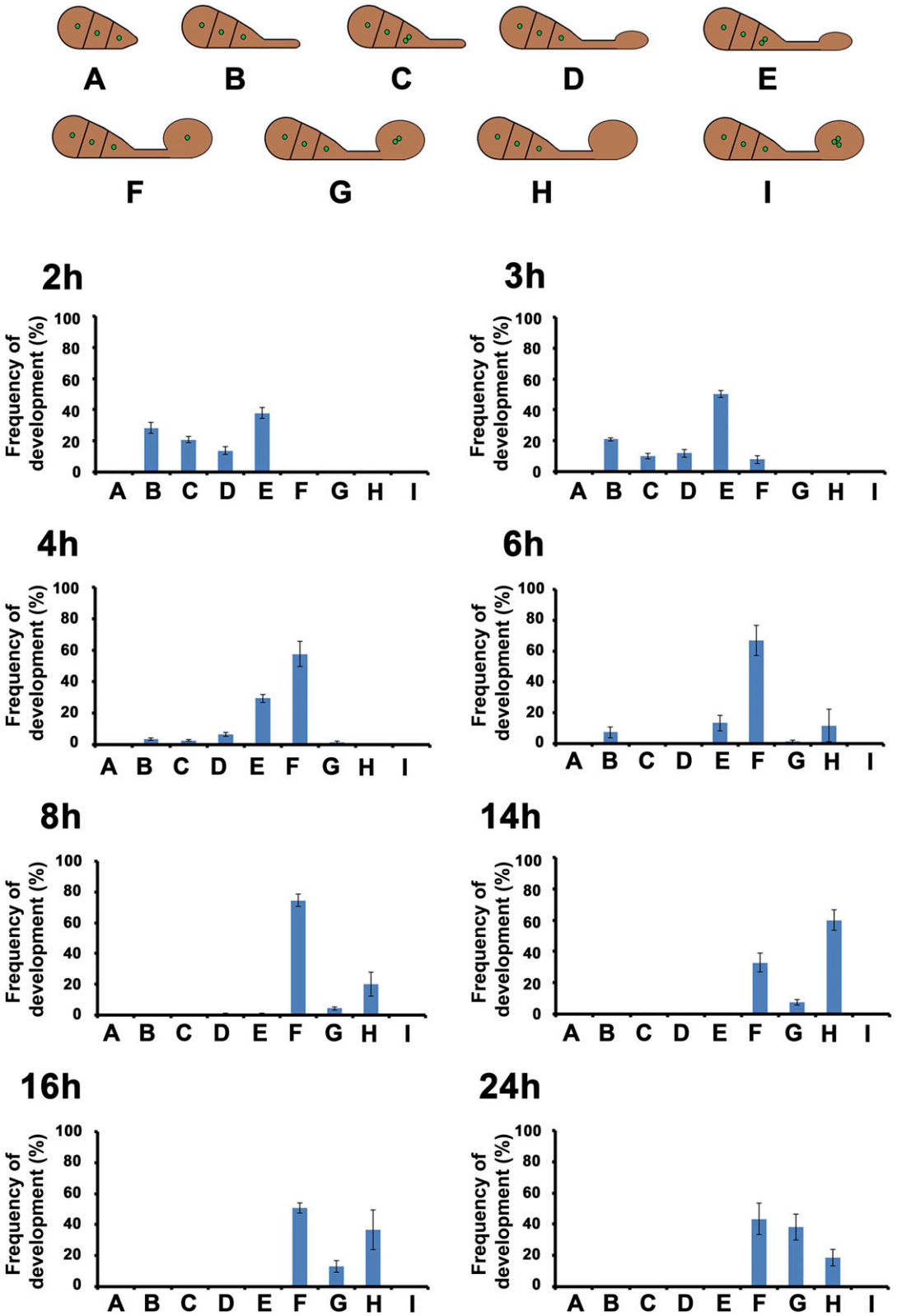

Fig. S1. Cell-cycle progression during appressorium development shown by GFP–LacI–NLS coexpressed with 256 repeats of LacO. (*Upper*) Diagram to show the stages of development during appressorium formation. Green dot depicts the fluorescence punctum resulting from GFP–LacI–NLS coexpressed with 256 repeats of LacO. One dot indicates the prereplicative stage (G1), and two dots indicate the postreplicative stage (S/G2). (*Lower*) Bar chart to show the frequency of developmental stages for each time point. Error bars represent the SD from three independent replicates of the experiment.

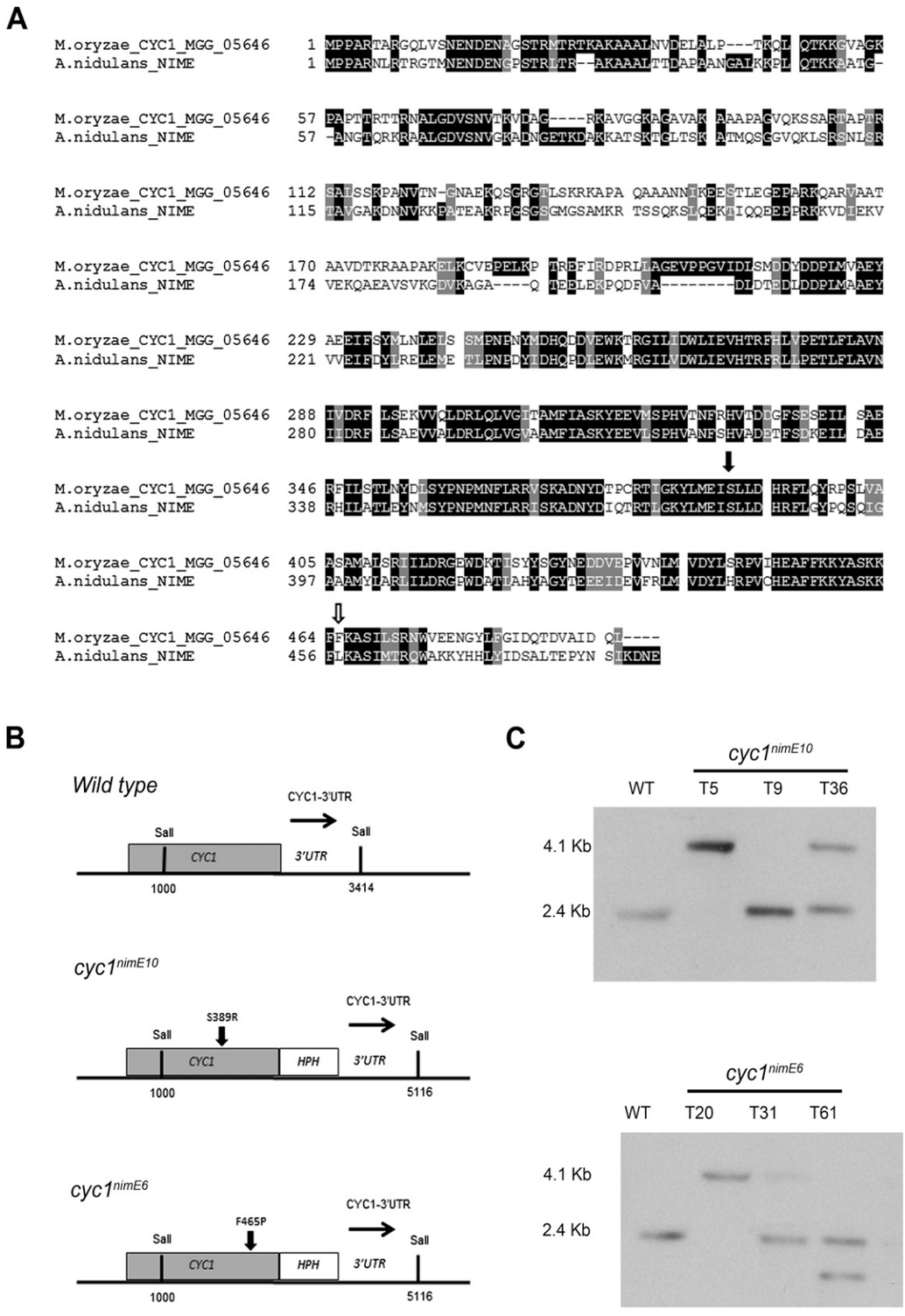

Fig. S2. Amino acid sequence alignment of the predicted *M. oryzae* Cyc1 and targeted gene replacement of *M. oryzae CYC1*. (*A*) The *NIME* locus of the wild-type, *nimE*10, and *nimE*6 *A. nidulans* strains was sequenced to show point mutations associated with temperature-sensitive alleles. Amino acid alignments were generated by using ClustalW2 and shaded by using Boxshade (Version 3.21). Numbers on the right indicate positions of amino acid residues. Amino acids shaded with a black background are identical among two fungi; dark-gray–shaded residues are similar in two of three; and those in white background do not show any similarity. The black arrow indicates the position of amino acid substitution of *cyc1*^{nimE10} (S389R), and the white arrow indicates that of *cyc1*^{nimE6} (F465P). (*B*) Schematic diagram indicates gene replacement strategy of *cyc1*^{nimE10} and *cyc1*^{nimE6} alleles. (*C*) Southern blot analysis to show the successful replacement of temperature sensitive alleles of *cyc1*^{nimE10} (*Upper*) and *cyc1*^{nimE6} (*Lower*) alleles. The size difference observed in each blot is consistent with successful replacement of the gene with a construct containing the resistance cassette *HPH*. Genomic DNA of putative transformants and the wild-type Guy11 were digested with the SalI enzyme. After fractionation by gel electrophoresis, blots were probed with a restriction fragment comprising the 3′ UTR of *CYC1*.

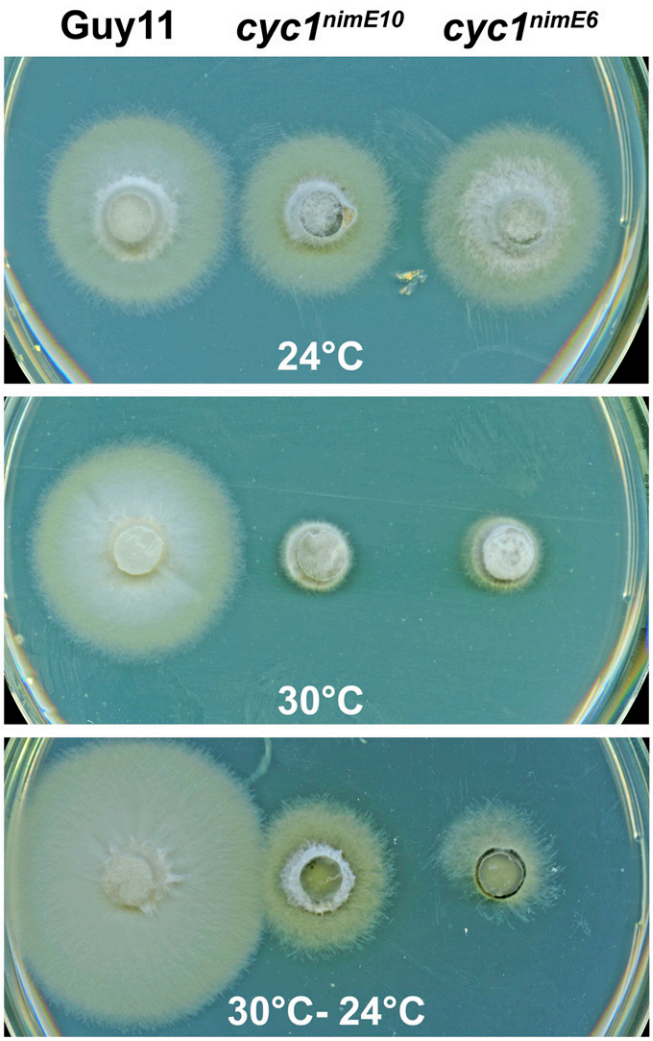

Fig. S3. Vegetative growth of Guy11, *cyc1*^{nimE10}, and *cyc1*^{nimE6} mutants at 24 °C and 30 °C. Plate cultures of mutants grown at the permissive temperature of 24 °C or nonpermissive temperature of 30 °C for 5 d are shown. Resumption of growth at the permissive temperature was observed by switching plates to 24 °C after 7 d.

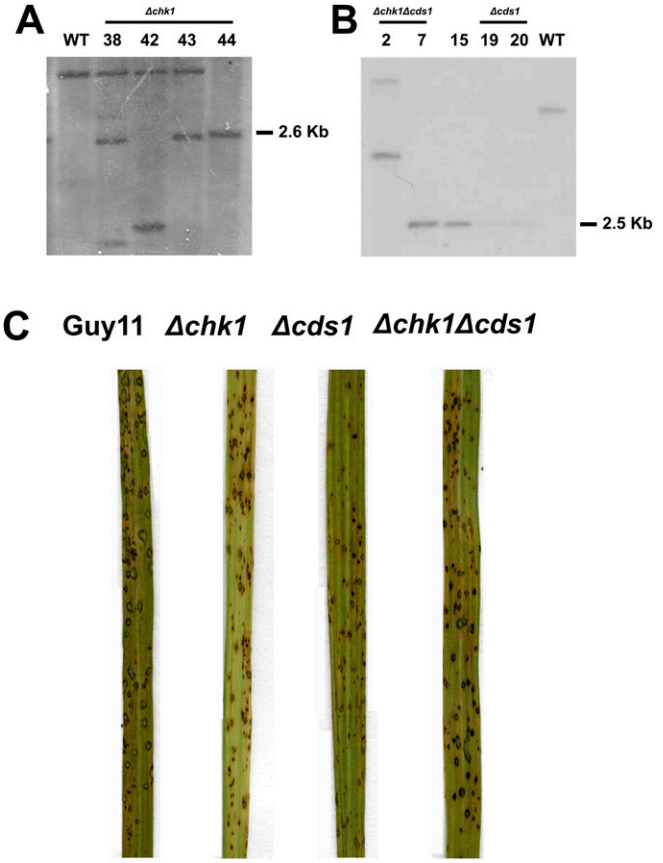

Fig. S4. Targeted gene replacement of *M. oryzae CHK1* in the Guy11 background, *M. oryzae CDS1* in the Guy11 background, and *M. oryzae CDS1* in the Δ*chk1* background. (*A*) Southern blot analysis was performed to determine whether targeted gene replacement of *CHK1* had taken place, introducing a PvuI restriction digestion, followed by probing with the 1-kb upstream region of *CHK1* (Chk1.LF). The result showed a 4.4-kb band, when no gene replacement occurred, and a 2.6-kb band when the corresponding resistance cassette was integrated at the *CHK1* locus. The Southern blot confirmed the positive result for T44. (*B*) Southern blot analysis showing PstI restriction digestion of genomic DNA, followed by probing with the 1-kb upstream region of *CDS1* (Cds1.LF). This process generated a 5.5-kb band when no gene replacement had occurred and a 2.5-kb band when the corresponding resistance cassette was integrated at the *CDS1* locus. Transformant numbers 2 and 7 correspond to the Δ*chk1* mutation; number 15 corresponded to an unrelated construct; and numbers 19 and 20 corresponded to the Guy11 genotype. (*C*) Pathogenicity assays of CO-39 rice leaves inoculated with Guy11, *Δchk1*, *Δcds1*, and *Δchk1Δcds1* mutants after 5 d postinoculation.

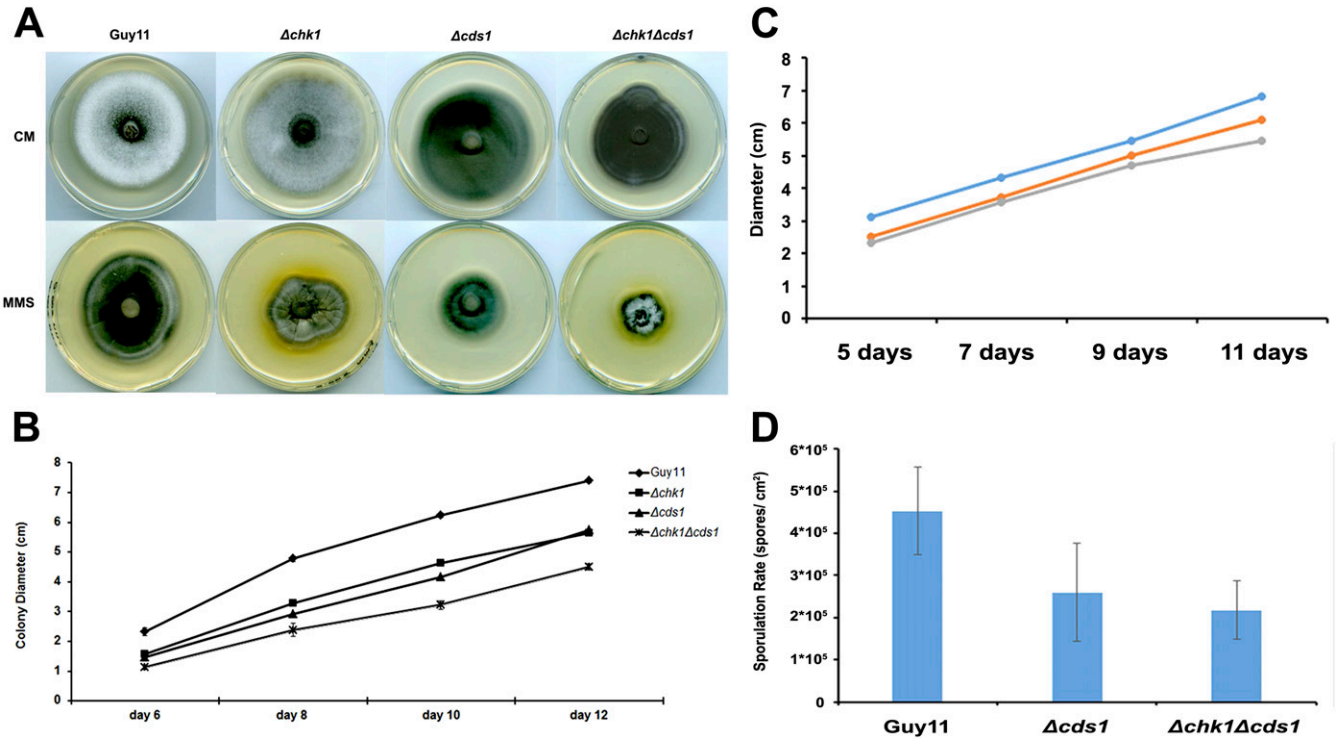

Fig. S5. Vegetative growth and colony morphology of DNA replication checkpoint mutants. (*A*) Mycelial plugs of Guy11, Δ*chk1*, Δ*cds1*, and Δ*chk1*Δ*cds1* mutants, respectively, were inoculated onto 0.001% of the alkylating agent methyl methanesulfonate (MMS) and in CM plates and incubated during 12 d at 26 °C. Images were taken by using an Epson Expression 1680 Pro scanner after 10 d postinoculation. (*B*) Colony growth of Guy11, Δ*chk1*, Δ*cds1*, and Δ*chk1*Δ*cds1* over the period of 12 d. Error bars represented the SE from three independent replicates. (*C*) Colony growth of Guy11, Δ*chk1*, Δ*cds1*, and Δ*chk1*Δ*cds1* mutants during a period of 12-d incubation in complete medium. Error bars represent the SE from three independent replicates. (*D*) Bar chart to show sporulation rate (spores per cm^2) of Guy11, Δ*cds1*, and Δ*chk1*Δ*cds1*. Error bars represented the SE from three independent replicates.

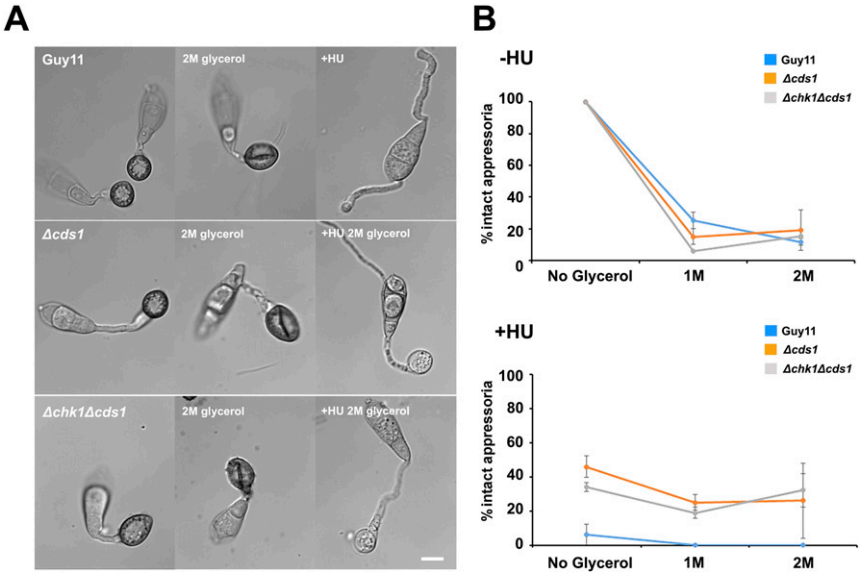

Fig. S6. *M. oryzae* DDR mutants develop nonmelanized appressoria in the presence of HU. (*A*) Micrographs to show the effect of 2 M glycerol with or without HU 200 mM when added to the appressoria of Guy11, Δ*cds1*, and Δ*chk1*Δ*cds1*. (Scale bar, 10 μm.) (*B*) Incipient cytorrhysis assay to measure appressorium turgor generation in *M. oryzae* mutants with or without HU. Conidia were allowed to germinate for 1 h, when 200 mM HU was added. At 24 h, appressoria were exposed to 1 and 2 M of glycerol concentration, and the percentage of intact appressoria was recorded (n = 2 experiments; appressoria observed = 64–165).

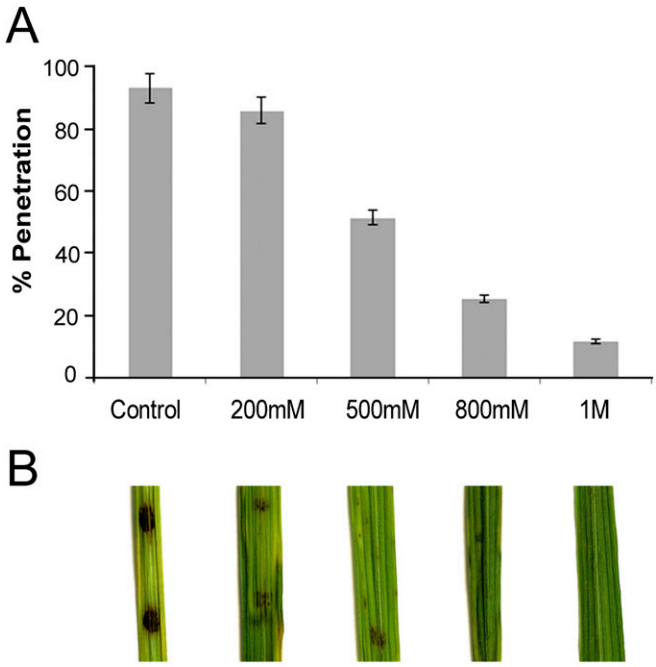

Fig. S7. HU blocks *M. oryzae* plant penetration in a dose-dependent manner. (*A*) Bar chart to show the effect of 200, 500, and 800 mM and 1 M HU concentrations on rice leaf sheath into 28-d-old CO-39 rice plants. HU was added at 10 hpi, and results were scored at 30 h ($n = 3$ experiments; appressoria = 50). (*B*) Effect of 200, 500, and 800 mM and 1 M HU concentrations on a leaf spot assay of wild-type Guy11 into 28-d-old CO-39 rice plants. HU was added at 10 h.

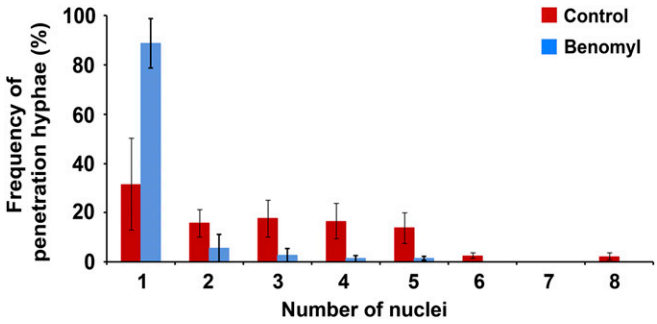

Fig. S8. Effect of benomyl treatment in the number of nuclei during plant penetration. Bar chart shows the frequency of penetration hypha development and the number of nuclei remaining in the appressorium after 30 hpi in the presence and absence of benomyl 50 $\mu g \cdot mL^{-1}$ when added at 10 hpi ($n = 3$ experiments; appressoria observed = 100).

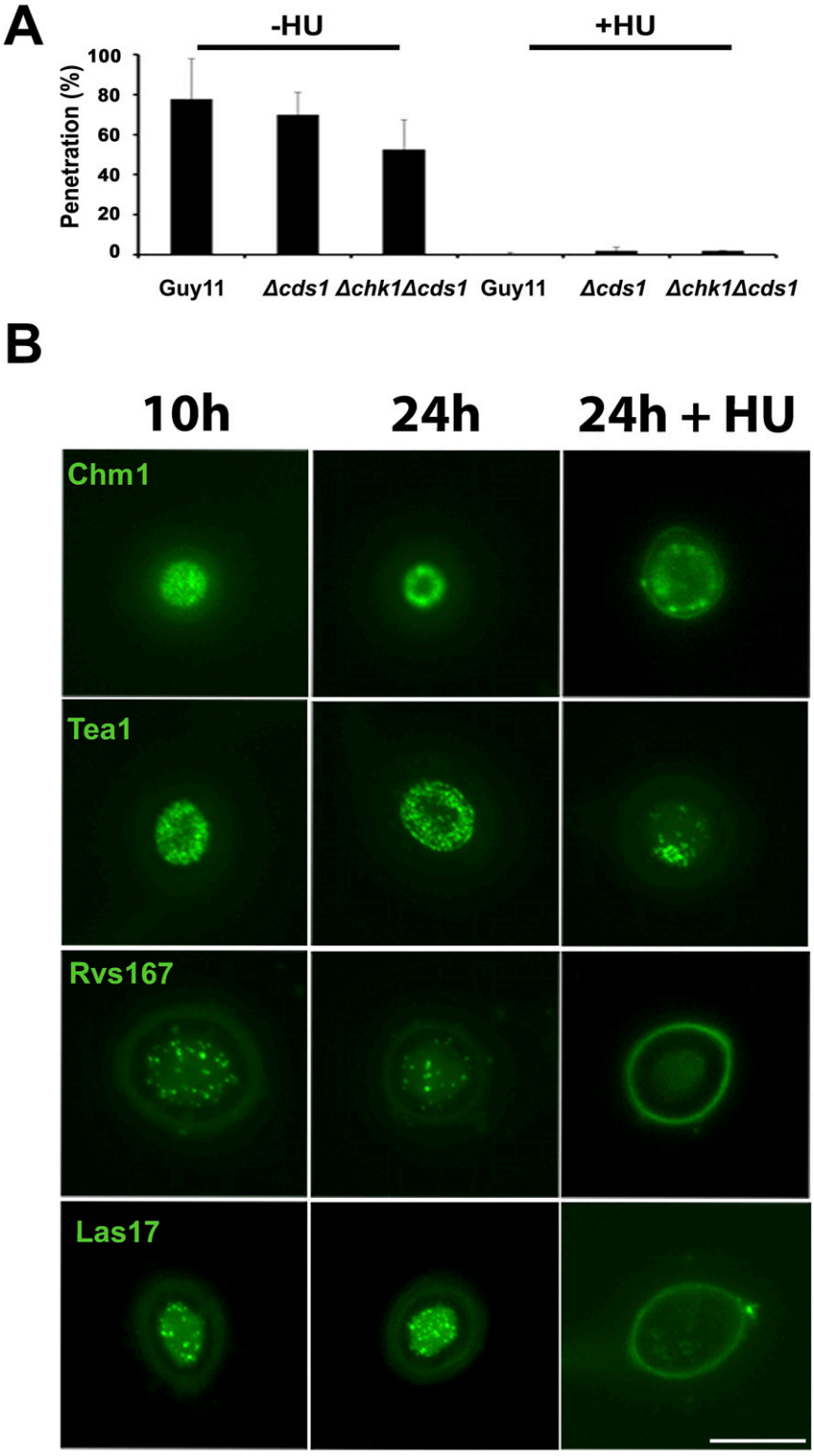

Fig. S9. S-phase regulation is independent of the DDR. (*A*) Involvement of DNA checkpoint kinases in appressorium-mediated plant penetration. Bar chart shows the percentage penetration of rice leaf sheath if cultivar CO-39 at 30 h inoculated with wild-type Guy11, *Δcds1*, and *Δchk1Δcds1* mutants at 30 h either with or without addition of 1 M HU at 10 h ($n = 3$ experiments; appressoria = 50). (*B*) HU affects localization of F-actin cytoskeleton-associated proteins during appressorium formation on glass coverslips. Micrographs show localization of Chm1–GFP, Tea1–GFP, Rvs167–GFP, and Las17–GFP during appressorium development at 10, 24, and 24 h when HU was added at 10 h. (Scale bar, 10 μm.)

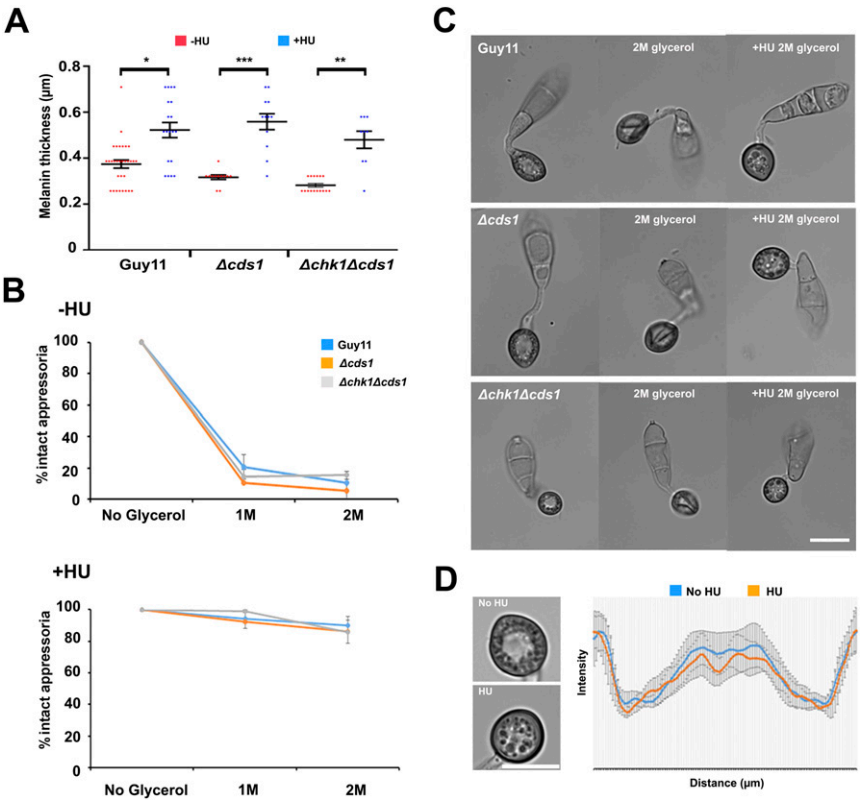

Fig. S10. Arrest in S phase increases melanin content and turgor generation of appressoria, independent of the DDR. (*A*) Arrest at S phase increases the thickness of the melanin layer, independently of the DDR. Scatter dot plot to compare melanin layer thickness after exposure to HU. Appressoria were allowed to form on hydrophobic plastic coverslips for 10 h, when 200 mM HU was added. At 24 h, micrographs were obtained to quantify the melanin layer thickness by measuring the intensity profile values over line scan diameters that crossed the center of the appressorium. $*P < 0.05$; $**P < 0.01$; $***P < 0.001$ (nonparametric Kruskal–Wallis test; $n = 2$ experiments; appressoria observed = 8–30). (*B*) Micrographs to show the effect of exposure to 2 M glycerol at 24 h, after addition of HU at 10 hpi in Guy11, Δ*cds1*, and Δ*chk1*Δ*cds1* mutants. (*C*) Incipient cytorrhysis assay to measure appressorium turgor generation in Guy11, Δ*cds1*, and Δ*chk1*Δ*cds1* mutants in the presence or absence of HU exposure (added at 10 hpi). Appressoria were allowed to form on hydrophobic plastic coverslips for 10 h, when 200 mM HU was added. At 24 h, appressoria were exposed to 1 and 2 M of glycerol concentration, and the percentage of intact appressoria was recorded ($n = 2$ experiments; appressoria observed = 84–134). (*D*) The pore was no longer formed in the presence of HU. Appressoria were allowed to form on hydrophobic plastic coverslips for 10 h, when 200 mM HU was added. At 24 h, micrographs were obtained to show absence of the appressorium pore when the inhibitor was added ($n = 3$ experiments; appressoria observed = 45). The graph shows the mean of intensity profile values overlaid (±SE) over 12-µm linescan diameter that crosses the appressorium through the center. (Scale bars, 10 µm.)

Table S1. Reciprocal shift experiment

Strains	Control	A	B	C	D	E	F	Cell phase
Guy11	98.2	95.1	95	91	0	94	93.2	No arrest
cyc1^{nimE10}	90	10	50	0	0	87	10.3	S
cyc1^{nimE6}	82	28.3	40.38	43.8	0	78	6	G2
nimA^{E37G}	88	40	80	29.4	0	81	0	G2

Reciprocal shift method was used to establish the arrest points of the cell cycle mutants (15). Conidia of the indicated strains were induced for appressorium development on coverslips and percentages of conidia in which appressorium maturation had occurred indicating completion of mitosis. At least 200 conidia were counted for each determination. Control, 24 h at 24 °C; A, 24 h at 29 °C; B, 8 h at 29 °C then 16 h at 24 °C; C, 8 h at 29 °C then 16 h at 24 °C with HU; D, 24 h at 24 °C with HU; E, 8 h at 24 °C with HU then 16 h without HU; F, 8 h at 24 °C, then 16 h at 29 °C without HU.

Table S2. Primers used in this study

Name	Sequence
NIME-P1	TTGGTGTTGCTGCCATGTTT
NIME-P2	AGGCAAAGTATCCCGGAGAC
V-BamHI-nimG11_P1	GCAGGCATGCAAGCTGGATCCCACAGACTTGTACACCGGACAAGA
Mut-nimG10_P2	GCGGATTTCCATGAGATACTTGCC
Mut-nimG10_P3	TATCTCATGGAAATCCGCCTTCTCGATCATCGCTTCT
Hyg-nimG10_P4	GGGAAAACCCTGGCGTCTCCTACAGCTGGTCGATAGC
Hyg-nimG10-3UTR_P5	AAATTGTTATCCGCTTTTGGATGGGAAGTTTTGGACC
V-BamHI-nimG10-3UTR_P6	TGATTACGCCAAGCTGGATCCGGACGATCACGACAAGCATAT
Mut-nimE6_P2	AGGGAATTTCTTGCTGGCATATTTCTT
Mut-nimE6_P3	AGCAAGAATTCCCTAAGGGTATGTTATCCGTCTCGT
M13F	CGCCAGGGTTTTCCCAGTCACGAC
M13R	AGCGGATAACAATTTCACACAGGA
CYC1-int-P1	CTACCCCAACCCCATGAACT
CYC1-int-P2	ACGTCTGTTTGGTCAATGCC
Chk1_50.1	GGGATGGTATATGGGCGTCTTG
Chk1_M13F	GTCGTGACTGGGAAAACCCTGGCGATTGCTGTACTTCGTAGGTCCGTT
Chk1_M13R	TCCTGTGTGAAATTGTTATCCGCTTCCCATTTCCAGGTCTGTAATAGT
Chk1_30.1	TTCCTCTTCCTCCTTATTTTTGCT
Cds1_50.1	TCAGCAGCCAACACATCTTTTTAC
Cds1_M13F	GTCGTGACTGGGAAAACCCTGGCGTCGTCACCATCCAGTCTAGCCT
Cds1_M13R	TCCTGTGTGAAATTGTTATCCGCTACATCTAAGCCGCGCATTGGAG
Cds1_30.1	TGGTTGCGGCTTATCTGGAGGC
HY split	GGATGCCTCCGCTCGAAGTA
YG split	CGTTGCAAGACCTGCCTGAA

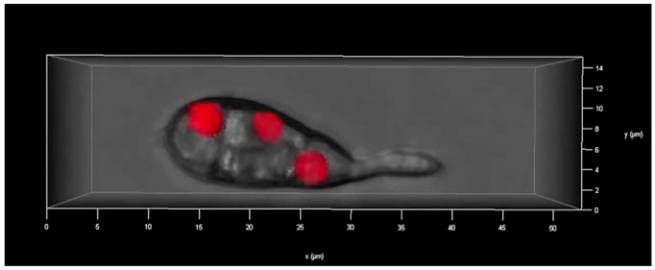

Movie S1. Live-cell imaging of cell-cycle progression during appressorium development in *M. oryzae*. Movie shows the Guy11 strain expressing H1-RFP during appressorium development germinated in hydrophobic coverslips during 24 h.

Movie S1

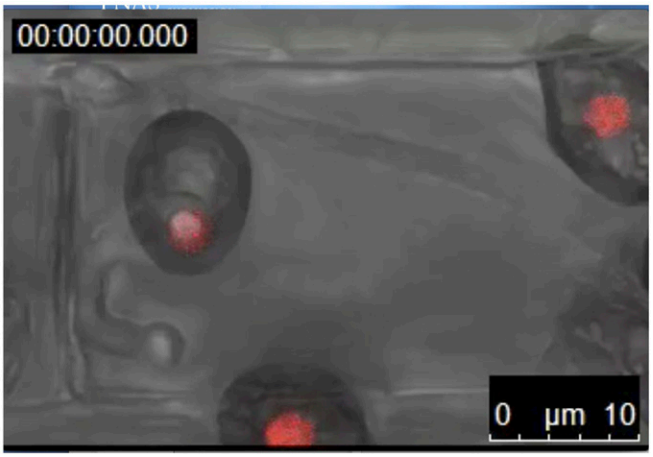

Movie S2. Live-cell imaging of cell-cycle progression during appressorium-mediated plant penetration in *M. oryzae*. Movie shows the Guy11 strain expressing H1-RFP during rice cuticle rupture and entry into the cell.

Movie S2